This is a preprint of: "Tails and bridges in the parabolic restricted three-body problem", Esther Barrabés, Josep Maria Cors, Laura Garcia-Taberner, Mercè Ollé, *Monthly Notices Roy. Astronom. Soc.*, vol. 472(3), 2554, 2017.
DOI: [10.1093/mnras/stx1990]

Tails and bridges in the parabolic restricted three-body problem

Esther Barrabés,[1]★ Josep M. Cors,[2]† Laura Garcia-Taberner[1]‡ and Mercè Ollé[3]§
[1] *Universitat de Girona, Escola Politècnica Superior, 17071 Girona, Spain*
[2] *Universitat Politècnica de Catalunya, Escola Politècnica Superior d'Enginyeria de Manresa, 08242 Manresa, Spain*
[3] *Universitat Politècnica de Catalunya, Escola Tècnica Superior d'Enginyeria Industrial de Barcelona, 08028 Barcelona, Spain*

ABSTRACT
After a close encounter of two galaxies, bridges and tails can be seen between or around them. A bridge would be an spiral arm between a galaxy and its companion, whereas a tail would correspond to a long and curving set of debris escaping from the galaxy. The goal of this paper is to present a mechanism, applying techniques of dynamical systems theory, that explains the formation of tails and bridges between galaxies in a simple model, the so called parabolic restricted three-body problem, that is, we study the motion of a particle under the gravitational influence of two primaries describing parabolic orbits. The equilibrium points and the final evolutions in this problem are recalled and we show that the invariant manifolds of the collinear equilibrium points and the ones of the collision manifold explain the formation of bridges and tails. Massive numerical simulations are carried out and their application to recover previous results are also analyzed.

Key words: celestial mechanics – galaxies: interactions – methods: numerical

1 INTRODUCTION

Gaia data release 1 has reported very recently the discovery of tails around the Large and Small Magellanic Clouds (a pair of massive dwarf galaxies) as well as an almost continuous stellar bridge between them (see Belokurov et al. (2017)). Actually, in the seventies, the observation of tails and bridges in multiple galaxies was already recorded. We mention the interacting pairs M51 and NGC 5195 or the pair of interconnected galaxies Arp 295 as two particular examples (see Toomre & Toomre (1972) and references therein). These papers argue that tails and bridges are just tidal relics of close encounters between two galaxies. In order to study the effects of the brief but violent tidal forces due to a close encounter between the galaxies, several authors have considered a very simple model: each encounter involves only two galaxies assumed to describe parabolic orbits, and each galaxy is idealized as just a disk of noninteracting test particles which initially orbit a central mass point. This model corresponds to the parabolic restricted three-body problem (the *parabolic problem* along the paper), assuming that the two point primaries are the galaxies describing parabolic orbits around their common center of mass.

There are several studies of the observable bridges and tails in galaxies. For instance, in Condon et al. (1993) show that galaxies UGC 12914 and UGC 12915 have a continuum bridge, that is thought to be due to the collision of the galaxies 2×10^7 years ago, considering that the orbits are nearly parabolic. In Günthardt et al. (2006), the authors consider the system AM1003-435, that is composed by two interacting galaxies. They studied the dynamical evolution of the encounter between the galaxies to conclude that they were moving in parabolic orbits. The N-body simulation of the orbits of stars in the galaxies shows bridges and tails. Also using the parabolic model, Namboodiri et al. (1987) studied the existence of bridges and tails in interacting galaxies depending on the circular velocity of the stars within the galaxies.

The parabolic model has also been used in the study of close encounters between disc-surrounded stars and the formation of planets. Pfalzner et al. (2005) studied the change of mass between stars when one or both of them are surrounded by a disc of low-mass particles. They concluded that, in the coplanar case, there were more change of particles between stars when the encounter was prograde. Fragner & Nelson (2009) studied the effect of parabolic encounters in the formation of Jovian-mass planets. They concluded that planets that have been formed after encounters are more massive and also have greater semimajor axes. Steinhausen et al. (2012) studied the influence on the initial density of

★ E-mail: barrabes@imae.udg.edu
† E-mail: cors@epsem.upc.edu
‡ E-mail: laura.garcia@imae.udg.edu
§ E-mail: Merce.Olle@upc.edu

the particles in the change of mass between star-disk encounters, concluding that the shape of the mass distribution has a high effect on the final outcome. Finally, Faintich (1972), considered a Sun-star-comet system to determine the effect of the stellar encounter on the trajectory of the comet, but considereding a hyperbolic model instead of a parabolic one.

The goal of this paper is, applying techniques of dynamical systems theory, to describe a mechanism that explains the formation of bridges and tails in the very simple model of the parabolic problem. Without trying to make a definition, a *bridge* would be an arm between the two galaxies, whereas a *tail* would correspond to a long and curving set of particles escaping from a galaxy. More precisely, along the paper, we show that the invariant manifolds of the equilibrium points of the parabolic problem, and those of the equilibrium points inside the collision manifolds are the clue to find out such mechanism. We do massive numerical simulations, considering both equal and unequal primaries, and we show the unambiguous appearance of bridges and tails, after the close encounter of the primaries. In particular, inspired in Toomre & Toomre (1972), we repeat some of their computations and conclude that our mechanism applies to their simulations (although in that paper, no mention of dynamical systems tools is done at all).

In Barrabés et al. (2015) we studied the main features of the parabolic problem only for the case of equal primaries. In the present paper, we consider the parabolic problem for any value of the mass parameter μ, where $1-\mu$ and μ, for $\mu \in (0, 1/2]$, are the masses of the two primaries in normalized units. First, we show the main features of the problem and second we show the mechanism that explains the formation of tails and bridges.

More concretely, in Section 2 we describe the parabolic problem and the main relevant properties. The parabolic problem is gradient-like due to the existence of a piecewise monotone function, called Jacobi function. This property allows to classify all possible final evolutions on the dynamics of the parabolic problem. On one hand, the flow of the system is extended when the primaries are at infinity, so the phase space is compactified in the time variable and we obtain what we call the *global* system. The equilibrium points of the global system and their invariant manifolds will be some of the main actors in the description of the dynamics of the problem. In particular, we show that the invariant manifolds of codimension 1 play a key role because they separate the different types of orbits, that is, they act as frontiers and divide the phase space in regions where the final evolution is either capture or escape. On the other hand, since we are interested in solutions that have close paths to the primaries (or even collide with them), the regularization of the equations in synodical coordinates is also performed (as far as the authors know, no paper dealing with the parabolic problem has ever considered regularized equations). There are two *collision* manifolds that correspond to a collision between the particle and each primary. Inside each collision manifold, there exist two cylinders of equilibrium points. These equilibrium points, and the associated stable/unstable invariant manifolds in the global system will be the remaining cast of actors in the paper.

Section 3 is devoted to show that the stable invariant manifolds associated with the collinear equilibrium points and the unstable manifold associated to the equilibrium points in the collision manifolds are responsible for the existence of bridges and tails. Some numerical explorations are performed and, in particular some results from Toomre & Toomre (1972) are recovered and discussed. Finally we draw some conclusions.

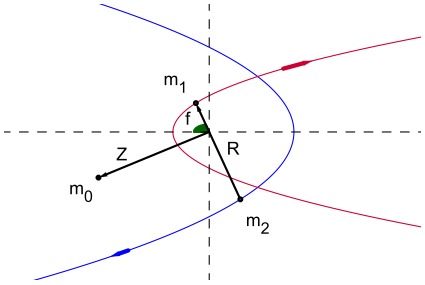

Figure 1. Parabolic problem in an inertial (sidereal) system of reference.

2 DESCRIPTION OF THE PROBLEM AND MAIN FEATURES

In this section we present briefly the equations of the motion of the parabolic problem and other main features. The details can be found in Alvarez et al. (2006) and Barrabés et al. (2015).

2.1 Equations of motion

Let be m_1 and m_2 be two bodies, called primaries, moving in parabolic orbits around their common center of mass. Consider a third body with infinitesimal mass moving under the gravitational attraction of the primaries in the same plane of the motion without affecting them. The planar parabolic restricted three body problem (simply *parabolic problem* along the paper) describe the motion of the infinitesimal mass.

We can consider, without loss of generality, suitable units of length and time, such that the constant of gravitation is equal to one and, the masses of the primaries are $m_1 = 1-\mu$ and $m_2 = \mu$, $\mu \in (0, 0.5]$ called the mass parameter. Then, the equation of the motion of an infinitesimal mass in an inertial system of coordinates $\mathbf{Z} = (X, Y)$, with origin located at the center of mass of the primaries, is given by

$$\ddot{\mathbf{Z}} = -(1-\mu)\frac{\mathbf{Z}-\mathbf{Z}_1}{|\mathbf{Z}-\mathbf{Z}_1|^3} - \mu\frac{\mathbf{Z}-\mathbf{Z}_2}{|\mathbf{Z}-\mathbf{Z}_2|^3}, \tag{1}$$

where $\mathbf{Z}_1 = \mu\mathbf{R}$ and $\mathbf{Z}_2 = (\mu-1)\mathbf{R}$, and $\mathbf{R} = (\sigma^2-1, 2\sigma)$ is the relative position vector from m_2 to m_1 where $\sigma = \tan(f/2)$, and f is the true anomaly, see Figure 1.

We perform two changes of variables. First, a rotating and pulsating (synodic) coordinate system $\mathbf{z} = (x, y)$, where the primaries remain fixed along the new x-axis at $\mathbf{z}_1 = (\mu, 0)$ and $\mathbf{z}_2 = (\mu-1, 0)$, given by the complex product

$$\mathbf{Z} = \mathbf{R}\mathbf{z} \tag{2}$$

and second, a change of time via $\frac{dt}{ds} = \sqrt{2}\,R^{3/2}$, where $R = |\mathbf{R}|$. The variable σ, that gives the relative position of the primaries, can be expressed in terms of the new independent variable (new time) s as $\sigma = \sinh(s)$. The primaries tend to infinity along their parabolic orbits, that is, when $t \to \pm\infty$, s also tends to $\pm\infty$.

Moreover, we can extend the flow of the system when the primaries are at infinity using a new variable θ introduced through the change $\sin(\theta) = \tanh(s)$. After straightforward computations, with the new variables $(\theta, \mathbf{z}, \mathbf{w} = \mathbf{z}')$, where $' = \frac{d}{ds}$ denotes the derivative with respect to s, the equation (1) becomes the following autonomous system (see Alvarez et al. (2006) for details)

$$\begin{cases} \theta' &= \cos\theta, \\ \mathbf{z}' &= \mathbf{w}, \\ \mathbf{w}' &= -A(\theta)\mathbf{w} + \nabla\Omega(\mathbf{z}) \end{cases} \tag{3}$$

where

$$A(\theta) = \begin{pmatrix} \sin\theta & 4\cos\theta \\ -4\cos\theta & \sin\theta \end{pmatrix}. \tag{4}$$

and

$$\Omega(\mathbf{z}) = x^2 + y^2 + \frac{2(1-\mu)}{\sqrt{(x-\mu)^2+y^2}} + \frac{2\mu}{\sqrt{(x+1-\mu)^2+y^2}}. \tag{5}$$

The extended phase space of system (3) is given by $D = [-\pi/2, \pi/2] \times (\mathbb{R}^2 - \{(-1/2, 0), (1/2, 0)\}) \times \mathbb{R}^2$, where the boundaries $\theta = \pm\pi/2$ represent the primaries at infinity. We will call system (3) the *global* system, and we denote as *configuration space* the projection of D on to the (x, y) plane. The two invariant systems $\theta = \pm\pi/2$ will be denoted as the *upper* and *lower* boundary problem respectively.

2.2 Equilibrium points, Homothetic solutions and the Jacobi function

All equilibrium points of the global system are points belonging to upper and lower boundary problems. As was shown in Alvarez et al. (2006), the equilibrium points of the parabolic problem in each boundary coincide with the classical five equilibrium points of the circular restricted three-body problem (see Szebehely (1967), for example): three collinear and two triangular. We denote by L_i^+ and L_i^-, $i = 1, ..., 5$, the equilibrium points for $\theta = \pi/2$, and $\theta = -\pi/2$ respectively. Along the paper, and in order to follow the same notation as in Alvarez et al. (2006) and Barrabés et al. (2015), we label the collinear equilibrium points increasingly with respect their location on the x axis: $x(L_1^\pm) < \mu - 1 < x(L_2^\pm) < \mu < x(L_3^\pm)$.

Linearizing the upper and lower boundary problems around the equilibrium points we obtain that collinear ones have an unstable manifold $W^u(L_i^+)$ of dimension 1 and a stable manifold $W^s(L_i^+)$ of dimension 3. In the case of triangular equilibrium points both invariant manifolds, unstable and stable, are of dimension 2. Considering the equilibrium points as a points in the global system (3), the dimension of $W^s(L_i^+)$, $i = 1, \ldots, 5$ increases by one. Using the symmetry of the problem

$$(s, \theta, x, y, x', y') \to (-s, -\theta, x, -y, -x', y'), \tag{6}$$

the invariant manifolds of the equilibrium points L_i^-, and their dimension, are obtained. See Table 1 and details in Alvarez et al. (2006).

Besides the equilibrium points, the simplest solutions of the global system (3) are the five homothetic solutions connecting the equilibrium points L_i^- with L_i^+, $i = 1 \ldots 5$, and belonging to $W^u(L_i^-) \cap W^s(L_i^+)$. Clearly these five homothetic solutions in the sidereal or inertial reference frame are solutions in which the three bodies (the infinitesimal mass and the two primaries) keep the same configuration all the time: either the three bodies lie in a line (collinear configuration) or they lie at the vertices of an equilateral triangle (triangular configuration).

	$L_{1,2,3}^+$	$L_{4,5}^+$
$\dim(W^u)$	1	2
$\dim(W^s)$	4	3

Table 1. Dimension of the invariant manifolds of the equilibrium points in the global system.

The parabolic problem also admits a function, similar to the Jacobi constant of the circular restricted three-body problem (see Szebehely (1967)), that we call, by similarity, the Jacobi function:

$$C = 2\Omega(\mathbf{z}) - |\mathbf{w}|^2. \tag{7}$$

Unlike circular problem C, in general, is not constant along the solutions of the global system (3), but it has a piecewise monotone behavior along the solutions, except at the homothetic solutions, where its value is constant. Precisely,

$$\frac{dC}{ds} = 2\sin\theta\,|\mathbf{w}|^2. \tag{8}$$

Therefore, along any solution of the global system C decreases when $\theta \in [-\pi/2, 0]$ $(s \le 0)$, whereas for $\theta \in [0, \pi/2]$ $(s \ge 0)$ the function C increases.

Given a value of C, let $V_0(C) = \{\mathbf{z} \mid 2\Omega(\mathbf{z}) = C\}$ be the set called zero velocity curves. Their topology is the same as in the circular restricted three body problem (see Szebehely (1967)). Let $C_i = C(L_i^\pm)$, $i = 1, \ldots, 5$, be the value of C at five equilibrium points. The so called Hill's regions, that is, the allowed regions of motion in the configuration space, can be obtained from (7). We plot in Figure 2 the zero velocity curves and the forbidden regions of motion (shaded regions) for different fixed values of C with $\mu = 0.4$.

We remark the fact that the zero velocity curves change with time: when $s \le 0$, the curves shrink and the Hill's region gets bigger, whereas for $s \ge 0$ the curves get bigger and the Hill's region decreases. This is a key factor for the description of the final evolutions of the solutions.

2.3 Final evolutions

Due to the geometry of the zero velocity curves and the nature of the Jacobi function, the behavior of the solutions as time tends to infinity are rather simple, mainly, escape and capture orbits. We use in the present paper the following definitions and results given in Barrabés et al. (2015). The results are valid for any value of μ. The proofs are similar to those given in Barrabés et al. (2015) for $\mu = 1/2$, so we do not repeat them here.

Definition 1. Let $\mathbf{Z}(t)$ be a solution of the parabolic problem given by equations (1). We say that

- it is a *capture* orbit around the primary of mass m_i, for $i = 1$ or 2, if $\limsup_{t\to\infty} |\mathbf{Z}(t) - \mathbf{Z}_i(t)| \le K$, for some constant K;
- it is an *escape* orbit if $\limsup_{t\to\infty} |\mathbf{Z}(t)| = \infty$ and $\limsup_{t\to\infty} |\mathbf{Z}(t) - \mathbf{Z}_i(t)| = \infty$ for $i = 1$ and 2.

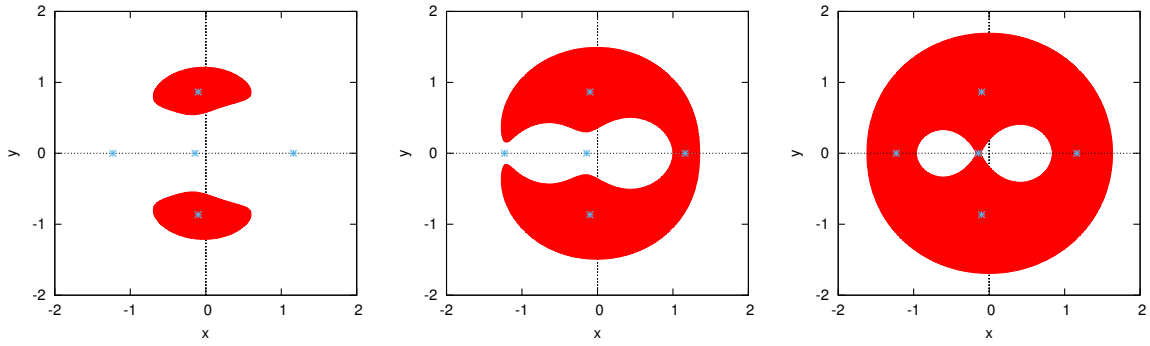

Figure 2. Zero velocity curves and the forbidden (shaded) regions of motion in configuration space for $\mu = 0.4$ and the fixed values of the Jacobi function $C = 6 < C_1$, $C = 7 \in (C_3, C_1)$, $C = 8 > C_2$ (from left to right). The location of the equilibrium points (although they do not leave at the same level of C) is also shown.

The definition of capture and escape is done in the inertial reference system. From the rotating and pulsating change of variables (2) we have that

$$|\mathbf{Z} - \mathbf{Z}_i| = R|\mathbf{z} - \mathbf{z}_i|, \tag{9}$$

where the distance between the primaries $R \to \infty$ as time tends to infinity. If an orbit escape in the synodic system z, then it will also escape in the inertial system. But notice that even if $\lim_{s\to\infty} |\mathbf{z}(s) - \mathbf{z}_i| = 0$, this is not sufficient to ensure capture in the sidereal system. In fact, it will be necessary to see that $|\mathbf{z}(s) - \mathbf{z}_i| = O(e^{-2s})$ when $s \to \infty$ (see Barrabés et al. (2015)). Due to that, we introduce the concept of a collision orbit in the synodic system.

Definition 2. Let $\gamma(s) = (\theta(s), \mathbf{z}(s), \mathbf{w}(s))$, $s \in [0, \infty)$, be a solution of the global system (3). We say that it is a *c*ollision orbit if $\liminf_{s\to\infty} |\mathbf{z}(s) - \mathbf{z}_i| = 0$, for some $i = 1, 2$.

Next two results state that the solutions of the global system belong to three disjoint classes and give us a classification criterium.

Proposition 1. (**Final evolutions**) Let $\gamma(s) = (\theta(s), \mathbf{z}(s), \mathbf{w}(s))$, $s \in [0, \infty)$, be a solution of the global system (3). Then, either it is a collision orbit, or $\lim_{s\to\infty} |\mathbf{z}(s)| = \infty$ or its ω-limit is an equilibrium point.

Proposition 2. (***C*-criterium**) Let $\mathbf{q} \in Int(D)$ with $\theta \geq 0$, and $\gamma(s) = (\theta(s), \mathbf{z}(s), \mathbf{w}(s))$, $s \in [0, \infty)$, the solution of the global system (3) through $\mathbf{q}$. Then,

(i) if for some time s_0 the value of the Jacobi function $C(\gamma(s_0)) > C_2$ and $\mathbf{z}(s)$ is located in one of the bounded components of the Hill's region, then it is a collision orbit;
(ii) if for some time s_0 the value of the Jacobi function $C(\gamma(s_0)) > C_1$ and $\mathbf{z}(s)$ is located in the unbounded component of the Hill's region, then it is an escape orbit.

For all values of μ, $C_1 < C_2$. Therefore, it is sufficient to monitor if $C(\gamma(s)) > C_2$ to be able to classify the orbit. In Table 2 we show the value of C_2 for the values of μ for which we will present some results in Section 3.

2.4 Regularization of the equations of motion

In order to study the collision with a primary and to deal numerically with orbits going close to the primaries, we need to remove the singularities $r_i = 0$, $i = 1, 2$ appearing in the equations of motion (3). In order to do so, we follow McGehee's ideas (see Pinyol (1995) for the elliptic RTBP and references therein) to obtain the so called regularized system of equations.

The regularization removes one singularity, $r_1 = 0$ or $r_2 = 0$ at a time. We describe here the procedure to remove the collision with m_1. We perform the following changes of variables:

(i) We move the selected primary m_1 to the origin:

$$(x, y, x', y', \theta) \to (X_1, X_2, X_3, X_4, \theta) \tag{10}$$

with $x = X_1 + \mu$, $y = X_2$, $x' = X_3$ and $y' = X_4$.
(ii) We proceed now with polar coordinates

$$(X_1, X_2, X_3, X_4, \theta) \to (r, \delta, \bar{y}, \bar{x}, \theta) \tag{11}$$

with $X_1 = r\cos\delta$, $X_2 = r\sin\delta$, $\bar{y} = r'$, $\bar{x} = r\delta'$.
(iii) We now consider

$$(r, \delta, \bar{y}, \bar{x}, \theta) \to (r, \delta, v, u, \theta) \tag{12}$$

with $v = \sqrt{r}\bar{y}$, $u = \sqrt{r}\bar{x}$.
(iv) Finally we introduce a new time variable τ by $\frac{ds}{d\tau} = r^{3/2}$.

After the computations to implement the above changes of variables and time, system (3) becomes

$$\begin{cases} \dot{r} = vr, \\ \dot{\delta} = u, \\ \dot{v} = \frac{1}{2}v^2 + u^2 - (v\sin\theta + 4u\cos\theta)r^{3/2} + 2r^3 + 2\mu r^2\cos\delta \\ \qquad - 2(1-\mu) - \frac{2\mu r^2}{r_2^3}(r + \cos\delta), \\ \dot{u} = -\frac{1}{2}uv + (4v\cos\theta - u\sin\theta)r^{3/2} + 2\mu r^2\sin\delta(-1 + \frac{1}{r_2^3}), \\ \dot{\theta} = r^{3/2}\cos\theta, \end{cases} \tag{13}$$

where $\dot{} = d/d\tau$ and $r_2 = \sqrt{r^2 + 2r\cos\delta + 1}$. We notice that this new system has only the singularity $r_2 = 0$.

We proceed in a similar way to remove the singularity $r_2 = 0$ from system (3), so the new associated system has only the singularity $r_1 = 0$. Along the integration of any

	$\mu = 0.5$	$\mu = 0.3$	$\mu = 0.1$
$L_2^{\pm}$	(0,0)	$(-0.2861297821, 0)$	$(-0.6090351100, 0)$
$C_2 = C(L_2^{\pm})$	8	7.840299166	7.193906458

Table 2. Position of equilibrium points $L_2^{\pm}$ and the value of $C_2 = C(L_2^{\pm})$ for three different values of μ.

given initial condition, we integrate numerically system (3) unless the particle is in a neighborhood of one of the primaries, where we apply the changes of variables and time and integrate the corresponding regularized system of equations.

2.5 The collision manifold

System (13) has an invariant manifold Λ_1 defined by $r = 0$, the so called *collision manifold* which corresponds to collision with the primary m_1 (similarly with m_2, we will obtain Λ_2). On Λ_1 there exist two cylinders of equilibrium points defined by

$$\begin{aligned} T^{\pm} =&\{(r, \delta, v, u, \theta) \in R^5 \,|\, r = 0,\ v = \pm v_0,\ u = 0, \\ &\delta \in [0, 2\pi], \theta \in [-\pi/2, \pi/2]\} \end{aligned} \tag{14}$$

with $v_0 = 2\sqrt{(1-\mu)}$.

In order to know the dimension of the invariant manifolds associated with each equilibrium point $P \in T^+$, we compute the Jacobian matrix M of the vector field of (13) at P and its spectrum:

$$Spec\, M = \{-\sqrt{1-\mu}, 2\sqrt{1-\mu}, 2\sqrt{1-\mu}, 0, 0\}. \tag{15}$$

There is an unstable 2D invariant manifold and a stable 1D one associated with each equilibrium point in T^+. Similarly each equilibrium point in T^- has associated 1D unstable and a 2D stable invariant manifolds.

Therefore the unstable (stable) invariant manifold associated with T^+ (T^-) is 4 dimensional. Along the simulations done in next Section, once we fix the value of the Jacobi function C and a particular value of θ, we will take a set of initial conditions that belong to T^+.

2.6 Dynamics of the parabolic problem

The dynamics of the parabolic problem can be understood focusing on its final evolutions (when time tends to plus/minus infinity) and looking for the heteroclinic connections between equilibrium points that exist in the upper and lower boundary problems. The interested reader can look at Figure 3 in Barrabés et al. (2015) where a map of connections in the upper boundary problem is shown.

The existence of only three different types of final evolutions becomes enriched due to existence of the homothetic solutions. Since they belong to $W^u(L_i^-) \cap W^s(L_i^+)$, they are a natural way to transport the dynamics near the lower boundary problem to the upper one. Moreover, in the case of the collinear equilibrium points, the invariant manifolds of codimension 1 behave as a frontier and divide the phase space in regions where only one of the other two final evolutions are allowed: escape or capture. We will see in Section 3 that these frontiers are also responsible of the existence of bridges and tails.

In order to emphasize the importance of the invariant manifolds of codimension 1 associated to the collinear equilibrium points, and how they separate the different type of orbits, we will reproduce some results from Section 4.2 in Barrabés et al. (2015) ($\mu = 0.5$ in that paper) for values of $\mu \neq 0.5$. More precisely, we take initial conditions at $\theta = 0$ in the plane (x, y'), that is, with $y = x' = 0$. These orbits are symmetric with respect to $\theta = 0$, so they have the same final evolution forwards and backwards in time. We integrate these initial conditions forward in time and classify the orbits using the C-criterium. Notice that due to the fact that some orbits can have a close encounter to a primary, a binary collision regularization is performed in order to continue the integration.

The detailed regions of escape and capture on the (x, y') plane are shown in Figure 3 for different values of μ.

Clearly, by Proposition 1, the frontiers between escape and capture regions must belong to $W^s(L_i^+)$ for a certain equilibrium point. As mentioned, the only stable manifolds of codimension 1 are those of L_i^+, $i = 1, 2, 3$. The frontier between two regions of capture orbits around different primaries correspond to $W^s(L_2^+)$, between an escape region and a capture around m_1 is $W^s(L_3^+)$ and between an escape region and a capture around m_2 is $W^s(L_1^+)$. To illustrate that, we consider the region $[-1.05, -0.9] \times [-4.2, -3.8]$, and a certain number of orbits in a circle of radius 0.05 around the point $x = -0.96$ and $y' = -3.88$. That point is close to a point where the three regions (capture around m_1, capture around m_2 and escape) meet. See Figure 4, left. In Figure 4 right, we show the evolution of the orbits, and we can see clearly that between the orbits that tend to m_1 (in red) and m_2 (in blue) there is one that belongs to $W^s(L_2^+)$; between the ones that tend to m_1 and escape (black), there is one that belongs to $W^s(L_3^+)$; and between the ones that tend to m_2 and escape, there is one that belongs to $W^s(L_1^+)$.

3 GENERATING BRIDGES AND TAILS

Our goal in this section is to show that the stable invariant manifolds associated to the collinear equilibrium points, $W^s(L_i^+)$, $i = 1, 2, 3$, and the unstable invariant manifold associated to the collision manifolds $W^u(m_i)$, $i = 1, 2$, are responsible for the existence of *bridges* and *tails*. First we perform a general and broad exploration considering big sets of initial conditions around a primary and we classify them depending on the final evolution of the orbits after the close encounter of the primaries. We show and comment the results obtained for $\mu = 0.5$, and then for $\mu \neq 0.5$. Second, we reproduce some explorations of Toomre & Toomre (1972). As we mention in the Introduction, our interest for the problem starts with their work, where the authors show that bridges and tails appear when the encounter of two galaxies is modeled by the parabolic problem. We show that their results can be

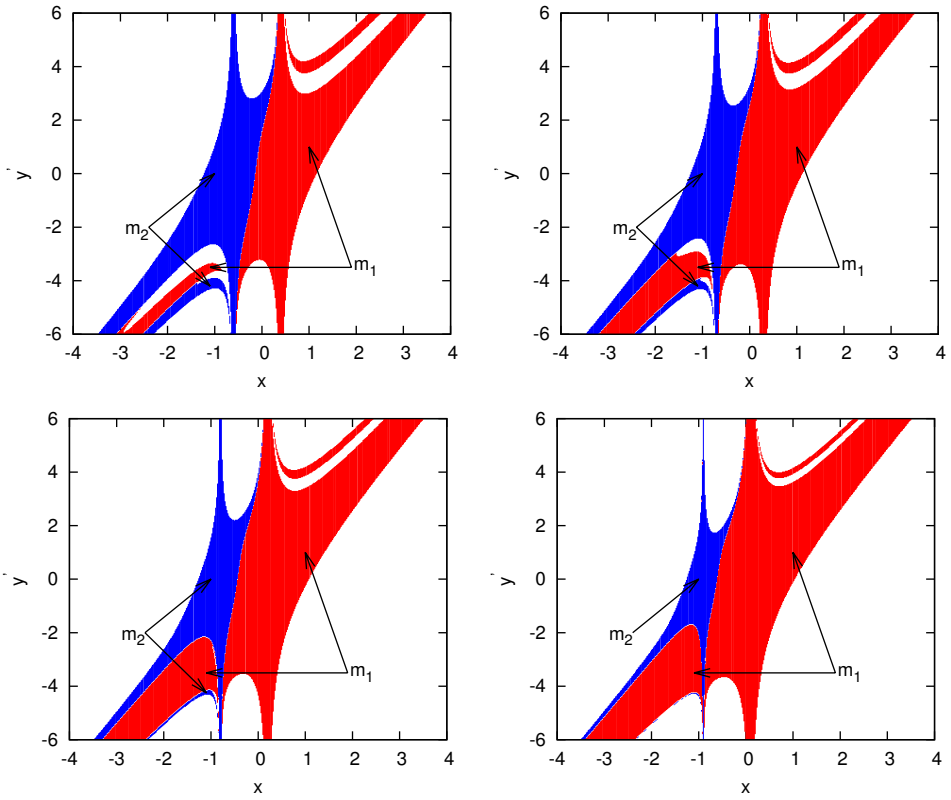

Figure 3. Regions of escape (white regions) and capture around m_1 (blue) and m_2 (red) in the (x, y') plane for $\mu = 0.4, 0.3, 0.2, 0.1$ from top to bottom, left to right.

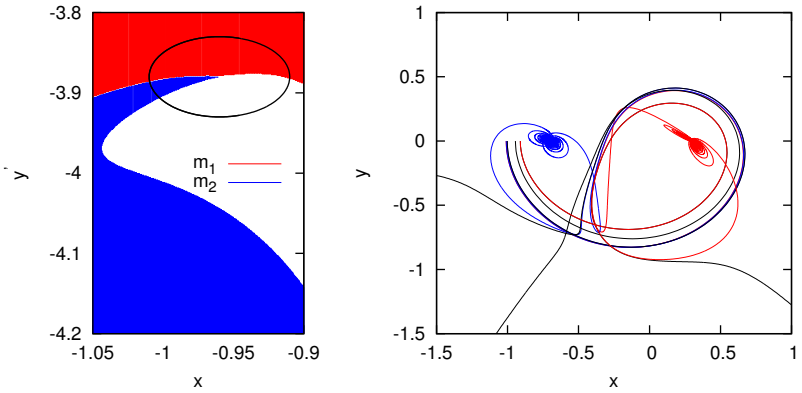

Figure 4. The left plot shows a magnification of the regions of capture around m_1 (blue) and m_2 (red) for $\mu = 0.3$. On the right plot, there are different orbits that escape, tend to m_1 or tend to m_2.

explained by the same dynamical mechanism that we study here.

The general exploration is performed as follows. First, we fix a negative value of $\theta = \theta_0$ (a time before the close encounter) and a value of $C \geq C_2$. For this value of C we know that the Hill's region has a bounded component around m_i (see Figure 2). Next, we take a circle centered at m_i and radius r_c such that it is contained in the bounded component of the Hill's region. Then, we generate a set of initial conditions (x, y, x', y') around the primary m_i as:

$$\begin{aligned} x &= x_{m_i} + r_c \cos\alpha & x' &= v\cos\beta \\ y &= r_c \sin\alpha & y' &= v\sin\beta \end{aligned} \tag{16}$$

where $x_{m_1} = \mu$ and $x_{m_2} = \mu - 1$, $\alpha, \beta \in [0, 2\pi]$ and v is obtained from (7). For any given α and β, we take the corresponding initial condition and we follow its trajectory, forward in time. Applying Proposition 2 each trajectory will be classified as a collision orbit with one of the primaries or an escape orbit.

For each fixed value of C and r_c, we take N equally spaced values of α and β. We show the results in two different ways:

• *Classification plots.* We plot in the (α, β) plane each point in different colors depending on the final evolution: red – captured by m_1, blue – captured by m_2 or white (blank) – escape.

• *Snapshots.* We plot the location of the particles in the configuration inertial frame (X, Y) for different values of time $\theta > 0$. The code of colors red and blue is the same one. The orbits that escape are plotted in black in these figures.

We will see how, considering different regions in the classification plots (and also for different values of r_c and C), the snapshots show the existence of bridges and tails.

Several comments regarding such initial conditions and the classification should be made. We observe that any negative value of θ_0 might be taken. The closer the value of θ_0 to zero, the smaller the distance between the primaries. We do not want to start too far from the closest passage between the primaries, nor too close. Moreover, any particle at a distance r_c of m_i in synodical coordinates, is at a distance $R_c = r_c R$ of that primary in the inertial frame, where $R = 1/\cos^2\theta_0$ is the inertial distance between the primaries. Thus r_c represents the ratio between the distance of the particle to the primary and the distance between the two primaries. We consider $\theta_0 = -\pi/4$, so $R = 2$, and $r_c \in (0, 0.2]$. Then, we have a set of initial conditions that forms an annulus that spreads around m_i up to 20% the distance between the two primaries in the inertial frame.

We also remark that the strategy to take such initial conditions inside the bounded component of the Hill's region guarantees, by the C-criterium, that all the trajectories considered eject from collision with m_i backwards in time. That is, all the trajectories considered belong to the unstable manifold of the collision with m_i, $W^u(m_i)$.

3.1 Results for $\mu = 0.5$

We take a set of test particles around one primary as in (16) with $\mu = 0.5$. Since both primaries have the same mass, it is enough to do the exploration only for one primary. We consider in this section all the particles leaving a neighborhood of m_1.

In Figure 5 we show the classification plots for $C = 8$ and several values of r_c. We have taken $N = 100$ (bigger values of N only convey to the same figures with more precision but the same information). On one hand, several mixed colored regions appear, specially as r_c increases. As mentioned before, all the orbits belong to $W^u(m_1)$, but forwards in time, different behaviors appear clearly: there exist orbits captured by m_1 or m_2 or escaping (red, blue and white colors respectively). On the other hand, it seems that there is a pattern **blue-red** for small r_c that disappears and gets more involved for bigger values of r_c. In particular, for r_c small the regions that correspond to escape orbits shrink, and in fact, for values r_c smaller than 10^{-3} we have not found escape orbits. That means that if a particle is too close to the primary (thinking in a galaxy, too close to the center) it has no time to escape (recall that for $\theta > 0$ the Hill's regions shrink; thus if a particle is in a bounded component and has a value $C > C_2$ at $\theta = 0$, it cannot escape). Clearly, the values of r_c for which there are no escape orbits depend on the value of θ_0 and C. In fact, similar patterns and results are obtained for different values of C: in general we find orbits tending to any of the primaries or escaping, except if r_c is too small. The bigger the value of C, the smaller the Hill's region around the primaries, and the less the probability to escape.

We now focus on the frontier separating the different colored regions. In Section 2.6, we showed that the codimension one stable manifolds of L_i^+, $i = 1, 2, 3$ separate different types of orbits and the points on the boundary between different colored regions (see Figure 3 and 4) precisely belong to $W^s(L_i^+)$, for a suitable $i = 1, 2, 3$. In a similar way now, we have that the points on the frontier separating the different colored regions that belong to $W^u(m_1)$, also belong to:

• $W^s(L_1^+)$ if the boundary curve separates a escape region (white) from a region of collision to m_2 (blue);
• $W^s(L_3^+)$ if the boundary curve separates a escape region (white) from a region of collision to m_1 (red);
• $W^s(L_2^+)$ if the boundary curve separates two different regions of collision (blue and red).

Therefore, the curves that separate two different regions belong to $W^s(L_i^+) \cap W^u(m_1)$, that is, they are *heteroclinic* orbits connecting a collision with m_1 and an equilibrium point.

Next we show that these heteroclinic orbits give simple mechanisms to explain tails and bridges. To do so, let us focus on selected ranges in the (α, β) plane where two different colored regions appear. We choose two zones: a red region (collision to m_1) surrounding a white one (escape region) (see the box in Figure 6, left), and a blue region (collision to m_2) surrounded by a red one (collision to m_1) (see the box in Figure 7, left). We also compute, using bisection method, the points on the frontier (thick black points).

Regarding the first zone, we focus on the separation points between escape and capture with m_1 – the black curve in Figure 6, left –, which correspond (integrating backwards and forwards in time) to heteroclinic orbits between m_1 and L_3^+. Close to these heteroclinic orbits, we have escaping orbits and orbits such that the particle remains captured by m_1. This is the mechanism that provokes the apparition of a tail. In Figure 6, right, we plot a snapshot at $\theta = 1.2$ of the location of the particles ((X, Y) in the inertial frame) with initial conditions (α, β) at the selected zone (the close encounter between the primaries has already taken place at $\theta = 0$). We observe the set of particles –red and black colour– that spread on a large region of the (X, Y) plane with the shape of a tail. As time tends to infinity ($\theta \to \frac{\pi}{2}$), some of them must remain around m_1, others must escape, and others must tend to the L_3^+ point (the thick curve in the right plot).

Concerning the second zone, the points belonging to the frontier between the two capture regions – blue and red –, that is the thick curve in Figure 7, left, correspond (integrating backwards and forwards in time) to heteroclinic orbits between m_1 and L_2^+. Similar to the previous case, as close to these heteroclinic orbits as desired, we have orbits such that the particle is captured by m_2 and orbits such that the particle is captured by m_1, when increasing the time (or θ). This is the mechanism that provokes the apparition of a bridge. In Figure 7, right, we plot a snapshot at $\theta = 1.2$ of the location of the particles ((X, Y) in the inertial frame) with initial conditions (α, β) at the selected region. We observe the set of particles connecting both primaries with the shape of a bridge. As before, when time tends to infinity ($\theta \to \frac{\pi}{2}$), some

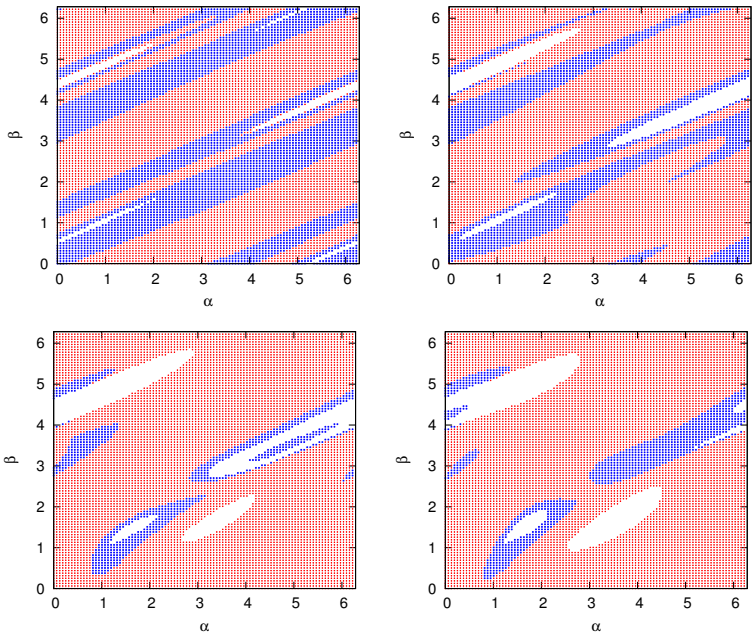

Figure 5. Classification of the final evolutions of the initial conditions (16) in the (α, β) plane for $C = 8$ and $r_c = 0.001, 0.01, 0.1, 0.2$ from top to bottom, left and right. Red and blue correspond to orbits tending to m_1 and m_2 respectively. White corresponds to orbits that escape. ($\mu = 0.5$)

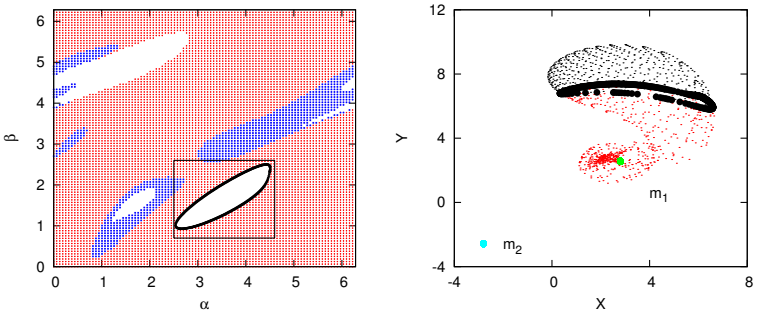

Figure 6. Left: classification plot of (α, β) points for $C = 8$ and $r_c = 0.2$. The rectangle shows the region where the initial conditions are taken (only points in the red and white regions). Right: snapshot for $\theta = 1.2$. Points on the $W^s(L_3^+)$ (thick black) are also plotted. ($\mu = 0.5$)

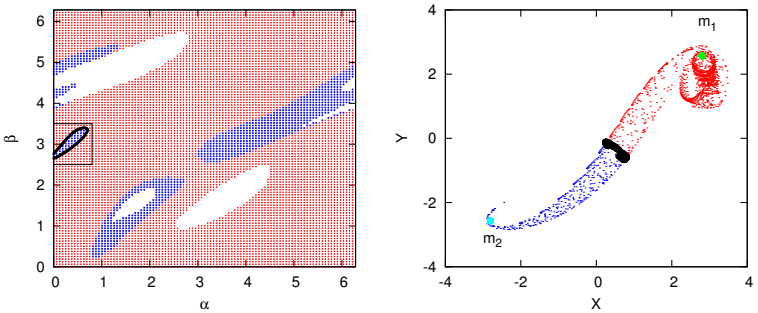

Figure 7. Left: classification plot of (α, β) points for $C = 8$ and $r_c = 0.2$. The rectangle shows the region where the initial conditions are taken. Right: snapshot for $\theta = 1.2$. Points on the $W^s(L_2^+)$ are also plotted. ($\mu = 0.5$)

of them must remain around m_1, others must transfer to a neighborhood of m_2 and remain around it, and others must tend to the L_2^+ point (the thick curve in the right plot is already close to L_2 for $\theta = 1.2$).

To show a bridge and a tail all together, we choose a suitable zone of initial conditions, for example $(\alpha, \beta) \in [5, 5.5] \times [3, 4]$, $r_c = 0.00405$ ($\simeq 1/100$ times the maximum r_c allowed by the zero velocity curve), and $C = 8$. In Figure 8 we plot the zone in the (α, β) plane considered (top left) and three different snapshots of the positions (X, Y) of each particle at $\theta = 0$, $\theta = \pi/8$ and $\theta = 1.2$. As explained above, the different colored layers of initial conditions will give rise to bridges and tails. We just remark that, due to the red thin layers between the white and blue regions in the classification plot shown in Figure 8, top left, the tail will be formed behind m_1, although in Figure 8, bottom right, it is apparently formed around m_2. As time increases, for $\theta > 1.2$, there will appear two new bridges (corresponding to the two thin red-blue transitions) as well as a tail behind m_1.

We emphasize that other values of $C \geq C(L_2) = 8$ might be taken. We have done the simulations for different values of C, ranging from 8 to 10, and for each fixed C, we have varied the value of r_c from 0 to 0.2 (or the maximum possible value defined by the bounded Hill region around m_1). We have observed that, as C increases, by (7) the modulus of the velocity for the initial conditions decrease. That means that for bigger values of the initial C, the particles have a smaller initial velocity, and also, the Hill's region is smaller, so they have a smaller chance to escape. In order to have quantitative estimates of the different types of orbits, we plot in Figure 9 the proportions of orbits captured by m_1, m_2 and escape with respect to the total of orbits computed, for different values of C. As expected, as C increases, a higher (lower) proportion of trajectories remaining captured by m_1 (escape) is obtained. Nevertheless, we see that there still are orbits escaping or being captured by m_2.

3.2 Results for $\mu < 0.5$

We take a set of test particles around both primaries as in (16) for different values of μ. The mechanism that explains the apparition of tails and bridges also applies, that is, for all the values of μ explored, we have always encountered heteroclinic orbits connecting the primaries m_i, $i = 1, 2$ with the collinear equilibrium points. The difference with the case $\mu = 0.5$ is that the primaries have different masses so we have to consider the influence of each primary separately and compute the corresponding proportions of orbits that tend to capture to each primary or escape.

Just as an example, in Figure 10 we show a snapshot for $\mu = 0.3$ where a bridge is clearly apparent, and a snapshot for $\mu = 0.1$ to show a bridge and a tail.

Following the procedure to obtain Figure 9, we have also computed the proportions of orbits captured by m_1, m_2 and escape with respect to the total of orbits computed, for different values of C (ranging in the interval $[C(L_2), 10]$) for different values of r_c and different values of μ. In Figure 11, we show the proportions of initial conditions of each type as C varies, for the values of $\mu = 0.5, 0.3, 0.1$. Since $C(L_2)$ varies with μ, we consider the normalized value $C/C(L_2)$. In order to compare the variation for different values of μ, we show the proportion of orbits captured by m_1 in the left plot, the proportion of orbits captured by m_2 in the center plot, and the proportion of orbits that escapes in the right plot. These proportions take into account if the particles are in a neighborhood of m_1 or m_2 before the close passage of the primaries (i. e., at the initial conditions for $\theta = -\pi/4$) –we will say that the particles *leave* m_1 or m_2, and of course, backward in time, they collide with m_1 or m_2–. The solid and dashed lines correspond to orbits that leave m_1 and m_2 respectively. The colors orange, violet and green correspond to $\mu = 0.5$, $\mu = 0.3$ and $\mu = 0.1$ respectively (labels in the plots have been added for black-white print).

As we can see from the left plot, for C close to (and bigger than) $C(L_2)$, the smaller the value of μ, the bigger the number of orbits captured by m_1 (assuming that the particles leave m_1 or m_2). However, when the particles leave m_2, the tendency in the proportion of capture orbits by m_1 is inverted when C increases, which seems reasonable because with bigger values of C, the Hill's region around m_2 shrinks with decreasing μ and there is a less possibility to leave the neighborhood of m_2.

From the center plot, an opposite behaviour can be observed for the proportion of capture orbits by m_2. For C close to (and bigger than) $C(L_2)$, this proportion decreases with μ (when leaving m_1 or m_2), but the tendency is inverted when C increases, that is the proportion increases with μ, just taking into account the particles that leave m_2.

Finally, taking into account both proportions of capture by the primaries, we obtain the right plot for the escape orbits. We observe, in particular, that given μ and for (suitable) big values of C, there are no escape orbits.

3.3 Toomre's explorations

As we mention in the Introduction, our interest for the problem starts with the work of Toomre & Toomre (1972), where the authors show that bridges and tails appear when the encounter of two galaxies is modeled by the parabolic problem. The authors consider a bunch of particles around one primary and far from the other primary. In this situation, the dynamics around the primary can be modeled by a two body problem (the influence of the second primary is a perturbation), so the particles can be considered orbiting in circular orbits around the primary in direct or retrograde motion. Then, the trajectories of all the particles are followed and their location in the inertial frame is plotted at different instants (what we have called snapshots). The authors observe the formations of bridges and tails, but they do not give a dynamical explanation on their formation.

We have seen that a dynamical explanation for bridges and tails comes from the existence of heteroclinic connections between collision with the primaries and the equilibrium points L_i^+, $i = 1, 2, 3$. Here we want to reproduce some explorations of Toomre and Toomre's paper in order to show that the initial conditions that they considered are close to these heteroclinic connections, so this is the reason why they see bridges and tails. We perform the explorations in two ways:

(i) Method 1 (TT_1): We consider initial conditions (x, y, x', y') as in (16) such that the sidereal velocity (X', Y') is perpendicular to the position vector (X, Y). To satisfy this restriction, for each value of α, only two values of β are ad-

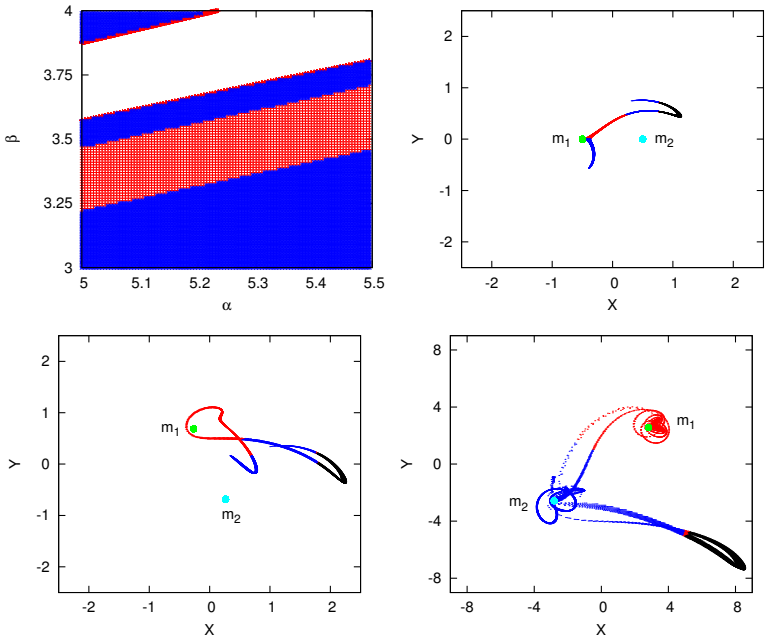

Figure 8. Top left: Detail in the (α, β) plane of the classification of the final evolutions of the initial conditions (16), for $C = 8$ and $r_c = 0.00405$. Top right and bottom: Positions in the inertial plane (X, Y) of a set of particles with initial conditions that correspond to orbits escaping, captured by m_1 or captured by m_2. The snapshots correspond to $\theta = 0$ (top right), and $\theta = \pi/8$ and $\theta = 1.2$ (bottom, respectively).

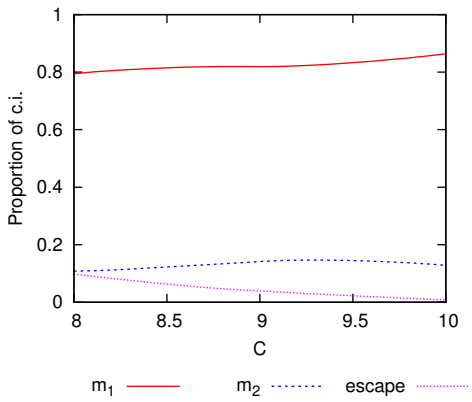

Figure 9. Proportions of orbits captured by m_1, m_2 and escape with respect to the total of orbits computed, for different values of C and $\mu = 0.5$.

missible:

$$\beta_{1,2}(\alpha) = \alpha \pm \arccos\left(\frac{\sqrt{2}}{v}(\mu(\sin\alpha + \cos\alpha) + r_c)\right). \tag{17}$$

This means that the initial conditions are at the apoapsis or periapsis of their orbits around the primary, although we do not ensure that the orbit is circular (thinking in a two-body problem m_1 plus a particle) because the modulus of the synodic velocity v is obtained from the fixed value of C. Nevertheless, the exploration done in this way allows us to compare the results with the ones previously obtained, because the initial value of C is fixed.

(ii) Method 2 (TT_2): We consider initial conditions (X, Y, X', Y')

$$\begin{aligned} X &= X_1 + R_c\cos\overline{\alpha}, & X' &= V\cos\overline{\beta}, \\ Y &= Y_1 + R_c\sin\overline{\alpha}, & Y' &= V\sin\overline{\beta}, \end{aligned} \tag{18}$$

such that $V^2 = 2(1-\mu)/R_c$ (velocity to ensure initial conditions on a circular orbit) and $\overline{\beta} = \overline{\alpha} \pm \pi/2$ (so the position with respect the primary (X_1, Y_1) and the velocity vectors are perpendicular); the $\pm$ sign refers to a direct/retrograde orbit.

In both methods, the synodical initial conditions are integrated until the orbit is classified according to its final evolution. As in the previous explorations, we take the initial conditions at $\theta_0 = -\pi/4$.

Concerning the results obtained from our simulations, we start first with method TT_1 with $\mu = 0.5$ and $C = 8$, varying r_c and $\alpha \in [0, 2\pi]$. In Figure 12, we show the classification plot for all values of α and β (see also Figure 5) and the curves $\beta_{1,2}$. We can see that the initial conditions considered overlap regions of different color, that is, there are orbits that will collide with m_1, or will collide with m_2 or that escape. Therefore, along the curves β_{12} there exit initial conditions belonging to heteroclinic connections between collision with m_1 and a collinear equilibrium point. So, following the mechanism described, tails and bridges appear, as was already shown in their paper.

Next, we repeat the exploration for the method TT_2. We fix a value of μ and a primary m_i. We take two sets of sidereal initial conditions for different values of R_c corresponding to direct and retrograde orbits. For each sidereal initial condition, we compute the corresponding synodic (x, y, x', y') initial condition for $\theta_0 = -\pi/4$ that can be written as in (16) with $r_c = R_c/2$, although now all of them have a different value of C. If any of those initial conditions has

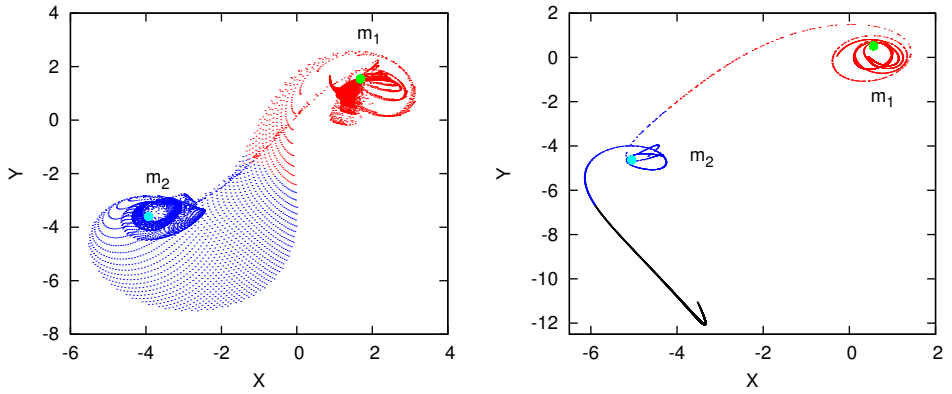

Figure 10. Snapshot to show a bridge for $\mu = 0.3$ (left) and both a bridge and a tail for $\mu = 0.1$ (right).

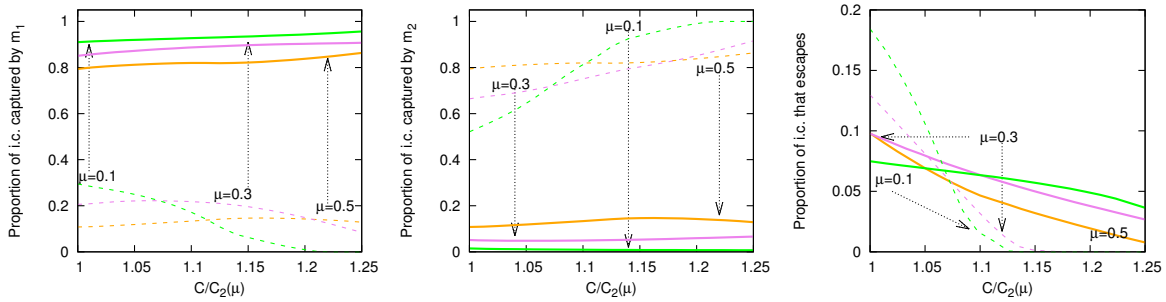

Figure 11. Proportions of orbits captured by m_1 (left), m_2 (center) and escape (right) with respect to the total of orbits computed, for different values of C and $\mu = 0.5$ (orange), $\mu = 0.3$ (violet) and $\mu = 0.1$ (green). Solid/dashed lines correspond to orbits leaving a neighborhood of m_1/m_2 respectively.

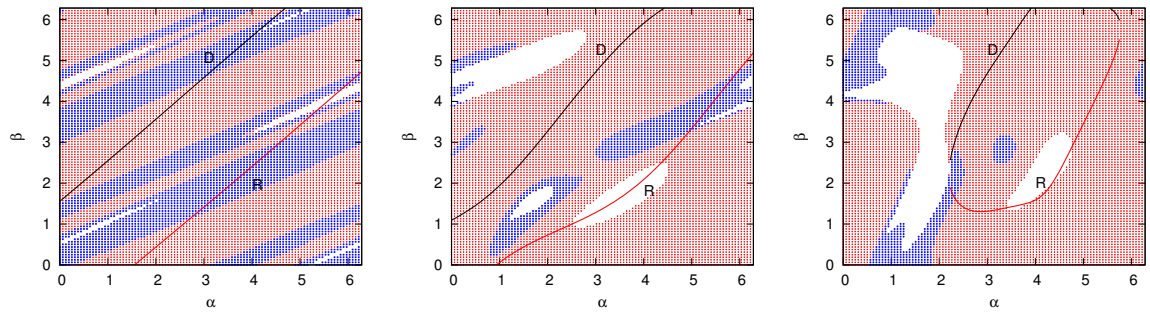

Figure 12. Classification plots of the method TT_1 in the (α, β) plane for $C = 8$ and $r_c = 0.001$, $r_c = 0.2$ and $r_c = 0.35$ (from left to right), and the curves $\beta_{1,2}$ (D stands for direct orbits, R for retrograde orbits). $\mu = 0.5$.

a value $C < 8$, it is discarded because we cannot ensure that it belongs to the collision manifold of m_1 (we only want to consider particles that backwards in time remain captured by m_1). Then, the orbits are followed until they are classified depending on their final evolution. Then we plot the initial conditions (X, Y) colored as follows: red if the orbit collides with m_1, blue if collides with m_2 and green if it escapes.

We show the results separately in four groups for initial conditions around m_1 or m_2, and for direct and retrograde orbits, for different values of μ. In each case, we show the results for the values of μ for which there are significant differences in order to see the evolution of the sets of collision orbits and escape orbits as μ decreases.

In Figure 13 we show the classification plots for direct orbits leaving a neighborhood of m_1. We see that only collision orbits with m_1 and escape orbits appear, and that as μ decreases, all the initial conditions correspond to collision orbits. Recall that the smaller the value of μ, the bigger the mass of m_1. Therefore, direct orbits only contribute to the formation of tails if μ is not too small.

In Figure 14 we show the classification plots for retrograde orbits leaving a neighborhood of m_1. In this case, for $\mu \geq 0.4$ we can see more richness, and bridges and tails with particles coming from m_1 appear. As μ decreases, again only collision orbits with m_1 are obtained.

In Figures 15 and 16 we show the classification plots for

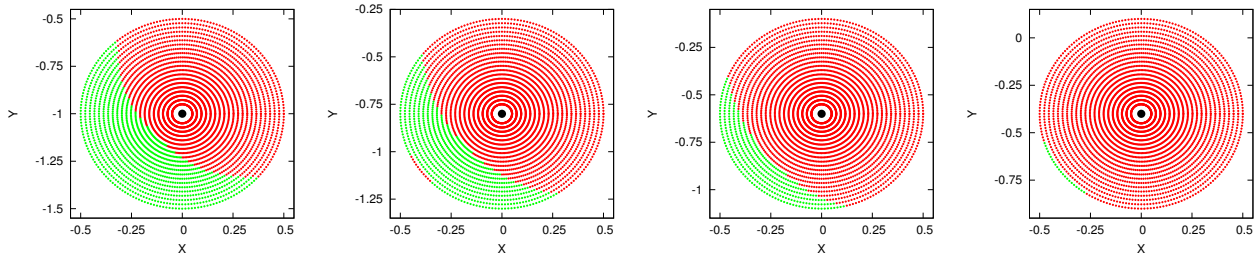

Figure 13. Results of the method TT_2. Initial conditions (X, Y) for *direct* orbits leaving a neighborhood of m_1 at $\theta_0 = -\pi/4$, classified depending on their final evolution. From left to right: $\mu = 0.5$, $\mu = 0.4$, $\mu = 0.3$ and $\mu = 0.2$.

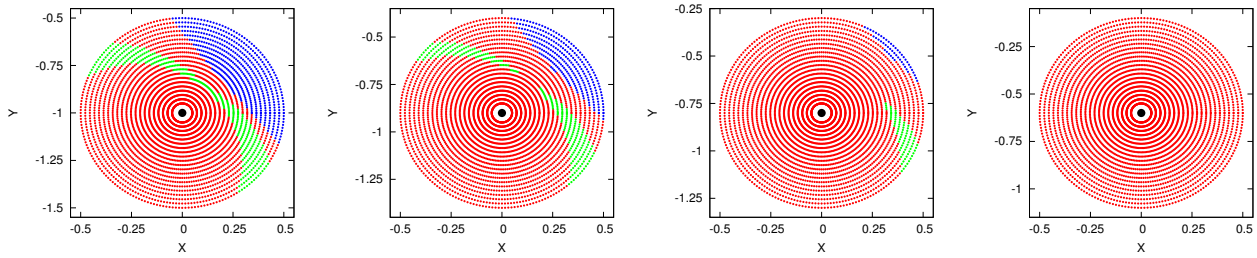

Figure 14. Results of the method TT_2. Initial conditions (X, Y) for *retrograde* orbits leaving a neighborhood of m_1 at $\theta_0 = -\pi/4$, classified depending on their final evolution. From left to right: $\mu = 0.5$, $\mu = 0.45$, $\mu = 0.4$ and $\mu = 0.3$.

direct and retrograde orbits, respectively, leaving a neighborhood of m_2. In the case $\mu = 0.5$ we obtain the symmetric plot of Figure 13 and 14 top left, due to the symmetry of the problem. As μ decreases, more diversity appears in both direct and retrograde orbits, and in particular the set of orbits that tend to m_1 grows. This can be explained simply by the fact that as μ decreases, m_1 gets bigger.

In summary, considering only circular orbits, we observe that the bridges are formed mostly by particles that leave a neighborhood of m_2. In particular, for $\mu = 0.5$, only the retrograde orbits coming from m_1 contribute to the formation of bridges. As μ decreases, the particles leaving a neighborhood of m_1 (in both direct or retrograde orbits) end colliding with m_1, whereas the particles leaving a neighborhood of m_2 experiment different final evolutions. However a big proportion of these initial conditions end at collision with m_1, so the attraction of m_1 after the close encounter is clearly apparent.

4 CONCLUSIONS

A dynamical mechanism that explains the formation of bridges and tails after a close approach of two galaxies when their motion is assumed to be parabolic is showed. Such an explanation is due to the existence of heteroclinic orbits between the collinear equilibrium points and the collision manifold associated to the primaries.

A classification of initial conditions that eject from one galaxy and after a close encounter will constitute a bridge or a tail is given. A more regular pattern appears when the initial conditions taken are closer to the galaxy.

The mechanism described has been applied to explain previous simulations on the formation of bridges and tails by other authors.

ACKNOWLEDGMENTS

E. Barrabés has been supported by grants MTM2013-41168-P and MTM2016-80117-P (MINECO/FEDER, UE), and AGAUR grant SGR1145. J.M. Cors has been supported by MINECO/FEDER grant MTM2013-40998-P, MTM2016-77278-P and AGAUR grant 2014 SGR 568. L. Garcia-Taberner and M. Ollé have been supported by the Spanish MINECO/FEDER grant MTM2015-65715-P and the Catalan grant 2014SGR-00504.

REFERENCES

Alvarez M., Cors J. M., Delgado J., 2006, Celestial Mech. Dynam. Astronom., 95, 173

Barrabés E., Cors J., Ollé M., 2015, Communications in Nonlinear Science and Numerical Simulation, 29, 400

Belokurov V., Erkal D., Deason A. J., Koposov S. E., De Angeli F., Evans D. W., Fraternali F., Mackkey D., 2017, Monthly Notices of the Royal Astronomical Society, 466, 4711

Condon J., Helou G., Sanders D., Soifer B., 1993, Astronomical Journal, 105, 1730

Faintich M., 1972, Celestial Mechanics and Dynamical Astronomy, 6, 22

Fragner M., Nelson R., 2009, Astronomy and Astrophysics, 505, 873

Günthardt G., Agüero E., Rodrigues I., Díaz R., 2006, Astronomy and Astrophysics, 453, 801

Namboodiri P., Kochhar R., Alladin S., 1987, Bull. Astr. Soc. India, 15, 186

Pfalzner S., Vogel P., ScharwÃd'chter J., Olczak C., 2005, Astronomy and Astrophysics, 437, 967

Pinyol C., 1995, Celestial Mech. Dynam. Astronom., 61, 315

Steinhausen M., Olczak C., Pfalzner S., 2012, Astronomy and Astrophysics, 538

Szebehely V., 1967, Theory of Orbits. The Restricted Problem of Three Bodies.. Academic Press, Inc.

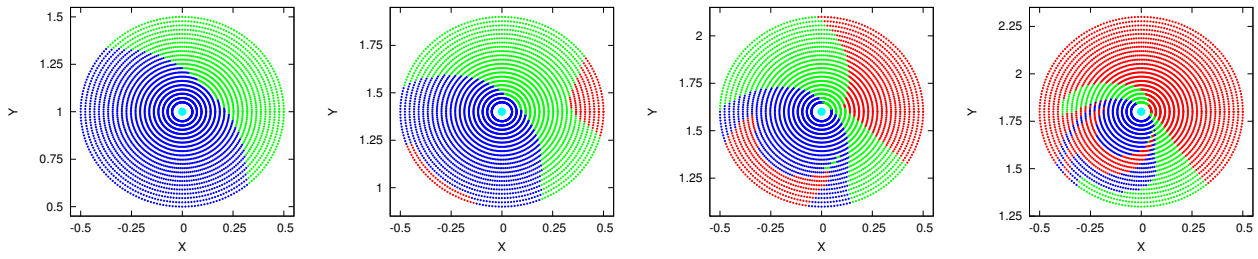

Figure 15. Results of the method TT_2. Initial conditions (X, Y) for *direct* orbits leaving a neighborhood of m_2 at $\theta_0 = -\pi/4$, classified depending on their final evolution. From left to right: $\mu = 0.5$, $\mu = 0.3$, $\mu = 0.2$ and $\mu = 0.1$.

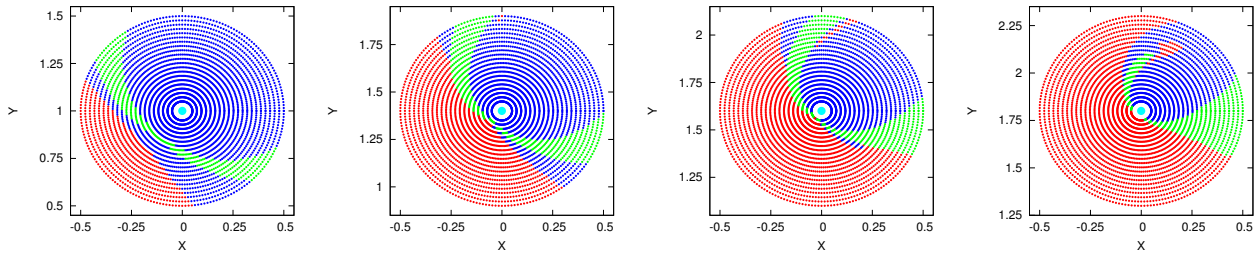

Figure 16. Results of the method TT_2. Initial conditions (X, Y) for *retrograde* orbits leaving a neighborhood of m_2 at $\theta_0 = -\pi/4$, classified depending on their final evolution. From left to right: $\mu = 0.5$, $\mu = 0.3$, $\mu = 0.2$ and $\mu = 0.1$.

Toomre A., Toomre J., 1972, The Astrophysical Journal, 178, 623